Coherent two-dimensional THz magnetic resonance spectroscopies for molecular magnets: Analysis of Dzyaloshinskii–Moriya interaction ⊘

Jiaji Zhang ✉ iD ; Yoshitaka Tanimura ✉ iD

Check for updates

CHORUS

🌐 View Online

↗ Export Citation

CrossMark

Coherent two-dimensional THz magnetic resonance spectroscopies for molecular magnets: Analysis of Dzyaloshinskii–Moriya interaction

View Online   Export Citation   CrossMark

Jiaji Zhang[a] (iD) and Yoshitaka Tanimura[a] (iD)

AFFILIATIONS

Department of Chemistry, Graduate School of Science, Kyoto University, Kyoto 606-8502, Japan

Note: This paper is part of the JCP Special Topic on Chiral Induced Spin Selectivity.
[a]Authors to whom correspondence should be addressed: zhang.jiaji.i92@kyoto-u.jp and tanimura.yoshitaka.5w@kyoto-u.jp

ABSTRACT

To investigate the novel quantum dynamic behaviors of magnetic materials that arise from complex spin–spin interactions, it is necessary to probe the magnetic response at a speed greater than the spin-relaxation and dephasing processes. Recently developed two-dimensional (2D) terahertz magnetic resonance (THz-MR) spectroscopy techniques use the magnetic components of laser pulses, and this allows investigation of the details of the ultrafast dynamics of spin systems. For such investigations, quantum treatment—not only of the spin system itself but also of the environment surrounding the spin system—is important. In our method, based on the theory of multidimensional optical spectroscopy, we formulate nonlinear THz-MR spectra using an approach based on the numerically rigorous hierarchical equations of motion. We conduct numerical calculations of both linear (1D) and 2D THz-MR spectra for a linear chiral spin chain. The pitch and direction of chirality (clockwise or anticlockwise) are determined by the strength and sign of the Dzyaloshinskii–Moriya interaction (DMI). We show that not only the strength but also the sign of the DMI can be evaluated through the use of 2D THz-MR spectroscopic measurements, while 1D measurements allow us to determine only the strength.

Published under an exclusive license by AIP Publishing. https://doi.org/10.1063/5.0156264

I. INTRODUCTION

Electron paramagnetic resonance (EPR) and nuclear magnetic resonance (NMR) have a long history as typical examples of two-dimensional (2D) spectroscopy techniques that measure the varying time intervals of magnetic pulse trains applied to electron or nuclear spin systems.[1,2] Although these techniques are powerful means for structural analysis of organic and inorganic materials, it is difficult to apply them to the investigation of spin dynamics because the time resolution of the magnetic pulses involved is limited to the order of microseconds.

Recently, coherent terahertz (THz) magnetic resonance (MR) spectroscopy was developed using magnetic pulses in the subpicosecond range generated by the magnetic-field component of THz light.[3–5] Just as ultrafast laser spectroscopy has made it possible to study the electronic excitation-state dynamics and intra- and intermolecular vibrational motions of complex molecular systems,[6] THz-MR spectroscopy has opened up the possibility of investigating strongly correlated spin dynamics in molecular magnets; this depends on the complex spin–spin interactions and the configurations of spins in the molecular environment, which cause dephasing and relaxation of the spin system.

The quasi-ferromagnetic (FM) and antiferromagnetic (AFM) precession modes in $YFeO_3$ (YFO) that arise from the antisymmetric spin–orbit coupling[7] have been observed as free induction decay (FID) signals.[8,9] Spin-wave excitation in AFM NiO has been detected with the aid of the Faraday effect.[10,11] The skyrmion, which is a quasiparticle composed of vortex-like spin orientations, has been detected in several FM and AFM materials with thin-film structures.[12–14] THz electron spin resonance (ESR) and Hall conductivity spectroscopy have been employed to investigate the topological Hall effect and phase transitions.[3,15–17]

Although THz-MR and THz-ESR spectroscopic approaches based on linear response theory have been successful for the classification of complex spin states in condensed phases,[18–20] it is unclear whether the spin states that are investigated are quantum-mechanically entangled and whether the width of the peaks that are measured arises from the relaxation or dephasing processes because

06 July 2023 00:51:49

these peaks are usually broad and overlap. Thus, an extension to coherent 2D THz-MR spectroscopy was developed. The observed 2D THz-MR spectrum for a YFO crystal made it possible to illustrate characteristic nonlinear spin responses, such as double-quantum (2Q) coherence and second-harmonic generation (SHG).[21]

As already illustrated in 2D optical spectroscopy,[22,23] 2D THz-MR spectroscopy is not only useful for identifying complex spin interactions but also for monitoring the complex quantum spin dynamics under the influence of relaxation and dephasing arising from the environment at the femtosecond scale. Theoretical input regarding the complex profiles of spin–spin interactions is important for analyzing these 2D spectra under ultrafast nonlinear processes. In particular, this includes those in molecular magnets, which play a central role in spintronics and next-generation information technologies.[24–26]

In this paper, we provide a comprehensive theoretical framework for both 1D and 2D THz-MR measurements based on the response-function theory developed for nonlinear optical spectroscopy techniques. To illustrate our approach more closely, we employ a chiral spin chain described as a Heisenberg model with exchange coupling and Dzyaloshinskii–Moriya interaction (DMI) arising from the antisymmetric spin–orbit coupling.[27–29] Such anisotropy of the spin system leads to a series of unique magnetic and optical properties.[30] Unlike conventional FM materials, in addition to the magnetic anisotropy, a non-centrosymmetric structure arises as the result of the chiral ordering of spins. As a result, a series of new phenomena arising from the nonlinear magnetic response, such as magneto-chiral dichroism and magnetization-induced SHG, were observed.[31–34]

To investigate the properties of such materials as devices, it is necessary to investigate ultrafast spin dynamics under time-dependent external fields, in which quantum coherence and entanglement—not only among spins but also between spins and the environment—play a significant role.[2,35] Thus, we include a harmonic heat bath of finite temperature in the spin system. The number of degrees of freedom of the heat bath is then reduced to obtain a time-irreversible equation of motion describing the effects of thermal fluctuations and dissipation.[36,37] Because the motion of the spins is much faster than the thermal noise arising from the heat bath, the heat bath must be treated in a non-Markovian manner. Thus, the reduced equations of motion derived using Markovian approximations and other assumptions—such as the Bloch, Lindblad, and Redfield equations—are not suitable for the description of such ultrafast spin dynamics. We then employ the numerically "exact" hierarchical equations of motion (HEOM) approach, which can be used to treat non-Markovian and non-perturbative system–bath interactions at finite temperatures.[38–41]

To demonstrate the applicability of the present theory, 1D and 2D THz-MR spectra were calculated for the chiral spin model with different DMI strengths describing the pitch and direction of chirality (clockwise or counterclockwise). We show that in 1D spectra, only the absolute strength of the DMI can be evaluated, whereas in 2D spectra, the sign of the DMI, which determines the direction of the chirality, can also be determined. While neutron-scattering techniques have been used to determine the structures of chiral materials, the present results indicate the possibility of determining the DMI through spin-dynamic processes. This finding should be valuable for the design of spintronic materials.

The rest of this paper is organized as follows: In Sec. II, we formulate linear (1D) and 2D THz-MR spectra based on the response-function theory. In Sec. III, we introduce the Heisenberg model with the DMI coupled to the harmonic heat bath. The HEOM is then presented. Numerical results and some discussion are presented in Sec. IV. Finally, Sec. V is devoted to our conclusions.

II. MAGNETIC SUSCEPTIBILITIES IN 2D THZ-MR SPECTROSCOPY

We consider a spin system coupled to a bath system driven by an external magnetic field $B(s)$. The total Hamiltonian is expressed as

$$\hat{H}'(s) = \hat{H}_{tot} + B(s)\,\hat{M}, \tag{1}$$

where $\hat{H}_{tot}$ is the Hamiltonian of a composite system and $\hat{M}$ is the polarization operator for magnetic fields.

The observable in a magnetic measurement at time t is expressed as $M(t) \equiv \langle \hat{M}(t) \rangle - \langle \hat{M} \rangle$, where $\hat{M}(t)$ is the Heisenberg representation of $\hat{M}$ for $\hat{H}'(s)$. The thermal average for any operator $\hat{A}$ is defined as $\langle \hat{A} \rangle \equiv \mathrm{tr}\{\hat{A}\hat{\rho}_{tot}^{eq}\}$, with the equilibrium density operator expressed as $\hat{\rho}_{tot}^{eq}$. We can also express this as $M(t) = \mathrm{tr}\{\hat{M}\mathcal{G}'(t)\hat{\rho}_{tot}^{eq}\} - \mathrm{tr}\{\hat{M}\hat{\rho}_{tot}^{eq}\}$, where the Liouville operator is defined as

$$\mathcal{G}'(t)\hat{\rho}_{tot}(0) \equiv \overleftarrow{\exp}\left[-\frac{i}{\hbar}\int_0^t \mathrm{d}s'\hat{H}'(s')\right]\hat{\rho}_{tot}(0)$$
$$\times \overrightarrow{\exp}\left[\frac{i}{\hbar}\int_0^t \mathrm{d}s'\hat{H}'(s')\right]. \tag{2}$$

Here, the arrows indicate time-ordered exponentials.

Experiments, such as 2D NMR and 2D EPS measurements,[1,2] are conducted using multiple magnetic pulses with finite time widths. In such experiments, the excitation by the external field is non-perturbative, and the desired spin dynamics are investigated by designing the profiles of pulse trains, as in the cases of spin-echo and correlation spectroscopy measurements. Theoretically, these signals are obtained by integrating the equations of motion for a spin system, such as the Bloch,[42] Redfield,[43] stochastic Liouville equations,[44] or the HEOM,[40,45,46] under a sequence of magnetic pulses.

As in the case of coherent optical laser spectroscopies, the excitations of coherent THz-MR spectroscopy are assumed to be impulsive, which allows us to measure the signals in different orders of the field-system interactions separately. Thus, we can employ a response-function theory developed for ultrafast nonlinear laser spectroscopy.[6] Up to the third order, the signal is then expressed as

$$M(t) = \int_0^t \mathrm{d}s\,\chi_1(s)\,B(t-s)$$
$$+ \int_0^t \mathrm{d}s_1 \int_0^{s_1} \mathrm{d}s_2\,\chi_2(s_1, s_2)\,B(t-s_1)\,B(t-s_2)$$
$$+ \int_0^t \mathrm{d}s_1 \int_0^{s_1} \mathrm{d}s_2 \int_0^{s_2} \mathrm{d}s_3\,\chi_3(s_1, s_2, s_3)$$
$$\times B(t-s_1)\,B(t-s_2)\,B(t-s_3), \tag{3}$$

where the linear, second-order, and third-order response functions are defined as[40]

$$\chi_1(s) \equiv -\frac{i}{\hbar}\langle[\hat{M}(s), \hat{M}]\rangle$$
$$= -\frac{i}{\hbar}\text{tr}\{\hat{M}\mathcal{G}(s)\,\hat{M}^{\times}\hat{\rho}_{tot}^{eq}\}, \quad (4)$$

$$\chi_2(s_1, s_2) \equiv -\frac{1}{\hbar^2}\langle[[\hat{M}(s_1+s_2), \hat{M}(s_1)], \hat{M}]\rangle$$
$$= -\frac{1}{\hbar^2}\text{tr}\{\hat{M}\mathcal{G}(s_2)\,\hat{M}^{\times}\mathcal{G}(s_1)\hat{M}^{\times}\hat{\rho}_{tot}^{eq}\}, \quad (5)$$

and

$$\chi_3(s_1, s_2, s_3) \equiv \frac{i}{\hbar^3}\langle[[[\hat{M}(s_1+s_2+s_3), \hat{M}(s_1+s_2)], \hat{M}(s_1)], \hat{M}]\rangle$$
$$= \frac{i}{\hbar^3}\text{tr}\{\hat{M}\mathcal{G}(s_3)\,\hat{M}^{\times}\mathcal{G}(s_2)\,\hat{M}^{\times}\mathcal{G}(s_1)\hat{M}^{\times}\hat{\rho}_{tot}^{eq}\}. \quad (6)$$

Here, $\mathcal{G}(s)$ is the Liouvillian without magnetic interaction, which is defined from $\mathcal{G}'(s)$ with $B(s) = 0$, and we have introduced the superoperator $\hat{M}^{\times}\hat{\rho} \equiv [\hat{M}, \hat{\rho}]$. The right-hand side (rhs) of the second line in each of the above equations allows us to employ the equations of motion to calculate the response functions and give us an intuitive picture of the higher-order optical processes.[40,41] For example, the rhs of the second line of Eq. (4) can be read from right to left as follows. The total system is initially in the equilibrium state $\hat{\rho}_{tot}^{eq}$. The initial state is then modified by the first magnetic pulses via the dipole operator as $(\hat{M}^{\times}\hat{\rho}_{tot}^{eq}) = [\hat{M}, \hat{\rho}_{tot}^{eq}]$ at $t = 0$ and is propagated for time $t = s$ by $\mathcal{G}(s)$. The expectation value is then obtained by calculating the trace of $\hat{M}$.

Actual 2D experiments have been conducted using a pair of magnetic pulses a and b with inter-pulse delay τ.[21,47] Under the impulsive approximation, the magnetic field is expressed as

$$B(s) = B_a\delta(s) + B_b\delta(s - \tau), \quad (7)$$

where B_a and B_b are the magnetic field strengths. The nonlinear element of the signal $M_{NL}(t, \tau)$ at $t + \tau$ is then evaluated as

$$M_{NL}(t, \tau) = M_{ab}(t + \tau) - M_a(t + \tau) - M_b(t + \tau), \quad (8)$$

where $M_{ab}(t + \tau)$, $M_a(t)$, and $M_b(t)$ are the total signal and the linear elements for pulses a and b, respectively.

From Eqs. (3) and (7), the nonlinear element is evaluated as

$$M_{NL}(t, \tau) = B_aB_b\chi_2(\tau, t) + B_aB_b^2\chi_3(\tau, 0, t) + B_a^2B_b\chi_3(0, \tau, t). \quad (9)$$

Thus, the characteristic features of THz-MR spectroscopy are described by the nonlinear susceptibilities. Because each term on the rhs has different proportionality with respect to B_a and B_b, they can be evaluated separately by changing their respective field strengths.

In nonlinear optical spectroscopies, χ_2 is used to analyze 2D THz-Raman[48,49] and 2D THz-IR-Raman signals[50,51] that involve a 2Q transition process, while $\chi_3(s_3, s_2, s_1)$ is used to analyze nonlinear 2D THz spectroscopies[52,53] including 2D THz rotational spectroscopy.[54,55] As illustrated in nonlinear optical spectroscopies, the s_1 and s_3 periods describe the time evolutions of coherent states, while s_2 describes the evolution of population states.[22,23] While

$\chi_3(\tau, 0, t)$ is used for 2D spectroscopies with waiting time $s_2 = 0$, $\chi_3(0, \tau, t)$ is used for transient absorption spectra in which the time evolution of the excited-state population is measured.

Using $\chi_1(s)$ in Eq. (4), the linear absorption spectrum is defined as

$$\chi_1(\omega) = \text{Im}\int_0^{\infty}\text{d}s e^{-i\omega s}\chi_1(s), \quad (10)$$

where Im denotes the imaginary part. Following the experimental setup, we consider two kinds of 2D spectrum for different time configurations of τ and t in Eq. (6), expressed as (1) $\chi_3(\tau, 0, t)$ and (2) $\chi_3(0, \tau, t)$. They are then expressed in the Fourier translation form as

$$\chi_3^{(1)}(\omega_\tau, \omega_t) = \text{Im}\int_0^{\infty}\text{d}\tau\int_o^{\infty}\text{d}t\,e^{-i\omega_\tau\tau - i\omega_t t}\chi_3(\tau, 0, t), \quad (11)$$

$$\chi_3^{(2)}(\omega_\tau, \omega_t) = \text{Im}\int_0^{\infty}\text{d}\tau\int_o^{\infty}\text{d}t\,e^{-i\omega_\tau\tau - i\omega_t t}\chi_3(0, \tau, t), \quad (12)$$

where ω_τ and ω_t represent the excitation and detection frequencies, respectively.[21]

III. CHIRAL SPIN MODEL AND HEOM APPROACH

To describe the novel phenomena of chiral magnets, we consider a linear chain system consisting of L spins. The system Hamiltonian is defined as

$$\hat{H}_S = J\sum_{n=1}^{L}\left[\hat{\sigma}_n^z\hat{\sigma}_{n+1}^z + \Delta\left(\hat{\sigma}_n^x\hat{\sigma}_{n+1}^x + \hat{\sigma}_n^y\hat{\sigma}_{n+1}^y\right)\right]$$
$$+ D_y\sum_{n=1}^{L}\left[\hat{\sigma}_n^z\hat{\sigma}_{n+1}^x - \hat{\sigma}_n^x\hat{\sigma}_{n+1}^z\right], \quad (13)$$

where $\hat{\sigma}_n^\alpha$ ($\alpha = x, y, z$) denotes the Pauli operator at the nth site in the αth direction. Here, the first term with $J > 0$ represents the AFM Heisenberg exchange coupling, and Δ is the anisotropic parameter. The second term in Eq. (13) is the DMI that is perpendicular to the xz plane, with coupling strength D_y. The sign of D_y determines the direction (i.e., clockwise or anticlockwise) or handedness (i.e., right- or left-handed circular configuration) of chirality, which is not easily determined by experimental measurements.[3,29] The magnetization operator is defined as

$$\hat{M} = \sum_{l=1}^{L}\hat{\sigma}_l^x. \quad (14)$$

A very important aspect of investigating ultrafast dynamics in magnetic materials is the inclusion of a quantum-mechanically consistent relaxation and dephasing mechanism. This can be achieved by including a harmonic heat bath in the spin system. The Hamiltonian of this heat bath is defined as

$$\hat{H}_B = \sum_j\left[\frac{\hat{p}_j^2}{2m_j} + \frac{m_j\omega_j^2}{2}\hat{x}_j^2\right], \quad (15)$$

where $\hat{p}_j$, $\hat{x}_j$, ω_j, and m_j represent the momentum, position, frequency, and mass of the jth oscillator, respectively. The system–bath interaction is defined by

$$\hat{H}_I = \hat{V} \sum_j g_j \, \hat{x}_j, \qquad (16)$$

where $\hat{V}$ represents the spin part of the system–bath interaction function, defined as

$$\hat{V} = \sum_n^L \hat{\sigma}_n^z, \qquad (17)$$

and g_j is the coupling strength with the jth oscillator. The total Hamiltonian is then given by

$$\hat{H}_{tot} = \hat{H}_S + \hat{H}_I + \hat{H}_B. \qquad (18)$$

In open quantum dynamics theory, the time-irreversible process can be described using a reduced set of equations of motion. After reducing the number of degrees of freedom of the heat bath, the noise effects are characterized by the correlation function,

$$C(t) = \frac{1}{\pi} \int_0^\infty d\omega J(\omega) \left[\coth\left(\frac{\beta\hbar\omega}{2}\right) \cos(\omega t) - i \sin(\omega t) \right], \quad (19)$$

where $J(\omega)$ is the spectral density function (SDF), $\beta = 1/k_B T$ is the inverse temperature, and k_B is the Boltzmann constant. For the heat bath, we assume the Drude SDF, which is expressed as

$$J(\omega) = \frac{\zeta \gamma^2 \omega}{\gamma^2 + \omega^2}, \qquad (20)$$

where ζ is the coupling strength and γ is the inverse correlation time.

In non-perturbative and non-Markovian conditions, the time evolution can be described by the HEOM approach.[38,39] We rewrite Eq. (19) in a linear-summation form,

$$C(t) = \sum_k^K c_k \, e^{-\nu_k |t|}, \qquad (21)$$

where c_k and ν_k are complex-valued coefficients. The HEOM can then be expressed as[40,41]

$$\frac{\partial}{\partial t} \hat{\rho}_{[\vec{n}]}(t) = -\left[i\hat{H}_S^\times + \sum_k^N n_k \nu_k \right] \hat{\rho}_{[\vec{n}]}(t) - i\hat{V}^\times \sum_k^K \hat{\rho}_{[\vec{n}+\vec{e}_k]}(t)$$
$$- i\sum_k^K \left[c_k \hat{V} \hat{\rho}_{[\vec{n}-\vec{e}_k]}(t) - c_k^* \hat{\rho}_{[\vec{n}-\vec{e}_k]}(t) \hat{V} \right], \qquad (22)$$

where $\vec{n} = \{n_1, n_2, \ldots, n_K\}$ denotes the index vector, and n_k are non-negative integers. Among all the $\hat{\rho}_{[\vec{n}]}(t)$, the zeroth, with $\vec{0} = \{0, 0, \ldots, 0\}$, corresponds to the density operator of the reduced system, while all the others are introduced for ancillary purposes.

In the HEOM approach, the response functions Eqs. (4)–(6) are evaluated as the time evolution of the system under external excitation. The density matrix is replaced by the HEOM elements, and the Liouvillian $\mathcal{G}(t)$ is replaced using Eq. (22).

For example, we can evaluate $\chi_3(\tau, 0, t)$ using the expression of the second line in Eq. (6) as follows.[40,41] We first run the

HEOM program for a sufficiently long period from a temporally initial condition at $t = -t_i$ [such as the factorized initial condition, $\hat{\rho}_{[\vec{0}]}(-t_i) = \exp[-\beta\hat{H}_S]$ with all the other hierarchy elements set to zero] to time $t = 0$ to reach a true thermal equilibrium, denoted by $\hat{\rho}_{[\vec{n}]}^{eq}(0)$. All the hierarchy elements have to be used to define a correlated initial condition. The system is next excited by the first magnetic interaction $\hat{M}$ at $t = 0$ as $\hat{\rho}'_{[\vec{n}]}(0) = [\hat{M}, \hat{\rho}_{[\vec{n}]}^{eq}(0)]$. The perturbed elements $\hat{\rho}'_{[\vec{n}]}$ then evolve in time by numerically integrating Eq. (22) up to t. At t, the system is excited by the second and third magnetic interactions as $\hat{\rho}''_{[\vec{n}]}(t) = [\hat{M}, [\hat{M}, \hat{\rho}'_{[\vec{n}]}(t)]]$. Then, after $\hat{\rho}''_{[\vec{n}]}$ evolves in time with the initial condition $\hat{\rho}''_{[\vec{n}]}(t)$ to $t + \tau$, the response function is calculated from the expectation value of the magnetic moment as $\chi_3(\tau, 0, t) = tr_A\{\hat{M}\hat{\rho}''_{[\vec{0}]}(t + \tau)\}$.

Notice that to take the system–bath coherence (or bath entanglement[41]) into account during the external perturbation, it is important to operate $\hat{M}$ to all of the hierarchy elements $\hat{\rho}''_{[\vec{n}]}(t)$. Although we only use $\hat{\rho}_{[\vec{0}]}(t)$ to calculate an expectation value, the other elements are essential to obtain an echo signal for non-Markovian noise in 2D spectroscopy.[40,41]

IV. NUMERICAL RESULTS

In the following, we set the exchange-coupling strength as the base unit $J = 1$ and calculate 1D (or linear absorption) and 2D spectra for $\Delta = 0.1$ as a model for typical AFM metal oxides.[56,57] The number of spin sites was $L = 6$, with periodic boundary conditions $\hat{\sigma}_n^\alpha = \hat{\sigma}_{n+L}^\alpha$. Here, we consider cases without the DMI ($D_y = 0$) and with the weak DMI ($|D_y| \leq 0.05$), which is appropriate for a small model system. Although the HEOM used in this study can investigate cases in which the system interacts strongly with the heat bath; here, we focus on the characterization of the chiral spin system and keep the coupling weak. Thus, the bath parameters were chosen as $\zeta = 0.05$, $\gamma = 1.0$, and $\beta\hbar = 10$. The hierarchy parameters were chosen as $K = 50$ and $\sum_k^K n_k \leq 10$, and the time step for numerical integration was set to $\delta t = 0.01$.

A. Energy eigenstates and transition elements of $\hat{M}$

To illustrate the origin of the peaks in the 1D and 2D spectra that will be shown later, in Table I, we present some representative energy eigenstates $|n_m^{(\prime)}\rangle$ that are necessary to explain THz-MR spectra. Here, $n = 0, 1$, and 2 represent the ground, first, and second excited states, respectively, and m and $\prime$ are introduced to signify the energy splitting arising from the anisotropic coupling Δ and the DMI, respectively. Thus, for example, the states $|1_0\rangle$ and $|1_0'\rangle$ are degenerate when $D_y = 0$. Note that to conduct numerical simulations, we employed all of the spin-z basis states to maintain numerical accuracy.

In Fig. 1, we depict the energy eigenstates (a) without the DMI ($D_y = 0$) and (b) with the DMI ($D_y = \pm0.05$). The possible magnetic transitions that arise from $\hat{M}$ are denoted by vertical arrows. Here, depending on the role of D_y, we classify the eigenstates as (I) independent of the DMI (black lines), (II) dependent on the square of D_y (blue lines), and (III) independent of the DMI but the phases of their wave functions change depending on the sign of D_y (red lines). For a finite D_y in Fig. 1(b), the degeneracy of eigenenergy is resolved

TABLE I. Eigenenergies of the spin Hamiltonian, $\hat{H}_S$: (a) without the DMI and (b) with the DMI.

	(a) $D_y = 0$	(b) $D_y = \pm 0.05$
$|0_0\rangle$	0	0
$|0_1\rangle$	0.001	0.001
$|1_0\rangle$	1.02	0.99
$|1_0'\rangle$	$\cdots$	1.14
$|1_1\rangle$	0.87	0.81
$|1_1'\rangle$	$\cdots$	0.98
$|1_2\rangle$	0.93	0.93
$|1_3\rangle$	1.15	1.15
$|2_0\rangle$	2.02	1.99
$|2_1\rangle$	2.03	2.03
$|2_2\rangle$	1.85	1.86
$|2_3\rangle$	2.02	2.02
$|2_4\rangle$	2.12	2.12

FIG. 1. Schematic view of the energy states of the spin Hamiltonian, $\hat{H}_S$: (a) without the DMI ($D_y = 0$) and (b) with the DMI ($D_y = \pm 0.05$). The black, blue, and red lines represent the states that are (I) independent of the DMI, (II) dependent on the square of D_y, and (III) independent of the DMI but the phases of their wave functions change depending on the sign of D_y, respectively. The purple arrows denote the possible transitions that arise from $\hat{M}$.

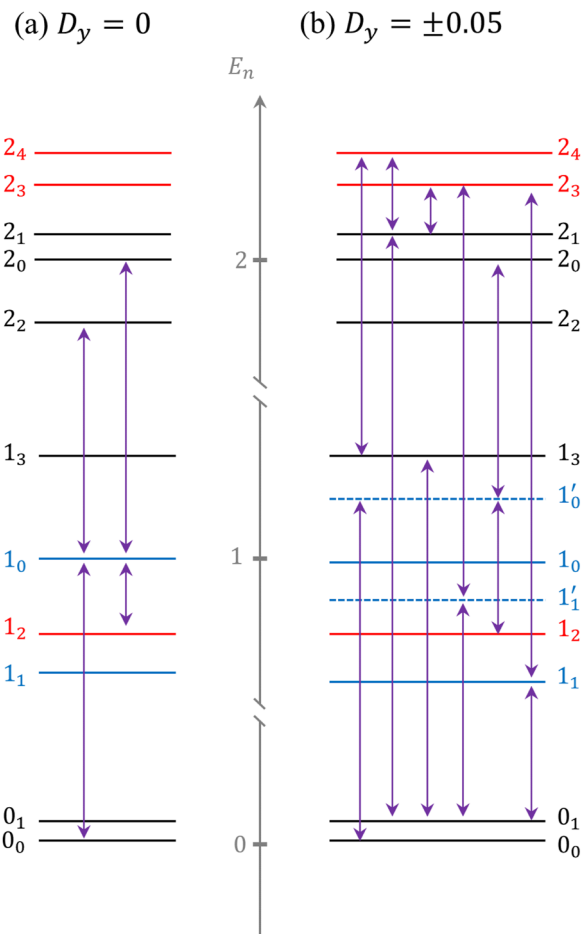because the inversion symmetry is broken, and we observe the finite energy gap in (II) (blue dashed lines).

B. 1D THz-MR spectrum

In Fig. 2, linear absorption (1D) spectra $\chi_1(\omega)$ calculated from Eq. (10) with Eq. (4) are presented for different D_y. Here, we only focus on $D_y > 0$ because the spectral profiles for $-|D_y|$ are identical to those for $+|D_y|$. The tiny symmetrical peaks around the main peak arise as an artifact of numerical Fourier transformation; these can be suppressed by increasing the time interval and introducing window functions.

Under current low-temperature conditions, the spin system is almost in the ground equilibrium states $|0_0\rangle$ and $|0_1\rangle$. The populations of other excited states are less than 0.1%, and we cannot observe the transitions from the excited states in the 1D spectrum. The main peak A_1 arises from the transition $|0_0\rangle \rightarrow |1_0\rangle$. Because the DMI resolves the degeneracy of states $|1_0\rangle$ and $|1_1\rangle$ (blue lines), the energy states $|1_0'\rangle$ and $|1_1'\rangle$ (blue dashed lines) appear for finite DMI, as illustrated in Fig. 1(b). Accordingly, we observe the adjoint peak A_2 that arises from the transition $|0_0\rangle \rightarrow |1_0'\rangle$. The energy eigenvalues of $|1_0\rangle$ and $|1_0'\rangle$ are (II) dependent upon the square of D_y, and we found that, for our system with $\Delta/J = 0.1$, these peak positions are evaluated as $\omega_{A_1} \approx -8.34 D_y^2 + 1.02$ and $\omega_{A_2} \approx 8.34 D_y^2 + 1.12$. Thus, from the position of the A_2 peak, we can estimate the magnitude of D_y, but we cannot determine the direction of chirality, which is described as the sign of D_y.

C. 2D THz-MR spectra

To elucidate the chirality of the system further, we next present numerical results for the 2D THz-MR spectrum evaluated from $\chi_3^{(1)}(\omega_\tau, \omega_t)$ and $\chi_3^{(2)}(\omega_\tau, \omega_t)$, expressed as Eqs. (11) and (12) with Eq. (6). In the present case, the rephasing parts ($\omega_t > 0$ and $\omega_\tau < 0$) in both 2D spectra have no signal, indicating that there is no spin echo.[22,23] Thus, we only present the non-rephasing parts of the spectra ($\omega_t > 0$ and $\omega_\tau > 0$).

1. Contribution from $\chi_3^{(1)}(\omega_\tau, \omega_t)$

In Fig. 3, we present contour maps of $\chi_3^{(1)}(\omega_\tau, \omega_t)$ in the (a) $D_y = 0$, (b) +0.05, and (c) −0.05 cases, in which the red and blue areas represent positive and negative intensities. To analyze the physical origin of each peak, we present a double-sided Feynman diagram corresponding to each labeled peak in Fig. 4(a). Here, the B_3 peak consists of two Liouville paths, which we denote as $B_3^{(i)}$ and $B_3^{(ii)}$.

These diagrams describe the time evolution of the left and right wave functions of the density operators involved in the response function from bottom to top under the magnetic excitations and deexcitations. For example, diagram $B_3^{(i)}$ in Fig. 4(a) describes the time evolution of the density operator undergoing magnetic interactions described by the purple arrows in Fig. 1 with the left wave function at time $s = 0$, $s = \tau$, and $s = \tau + t$ with the right wave function at time $s = \tau$. The left wave function evolves with time
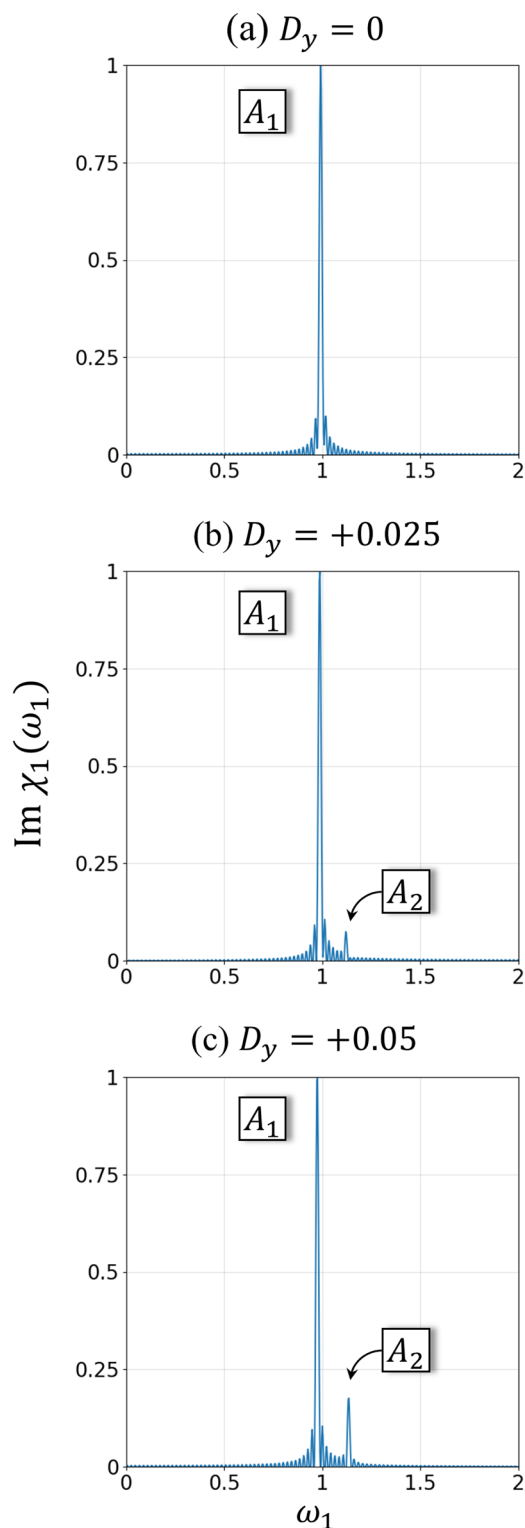
FIG. 2. Linear absorption (1D) spectra, $\chi_1(\omega)$ calculated for D_y = (a) 0, (b) +0.025, and (c) +0.05. The signal intensities are normalized with respect to the absolute values of the peak intensities.
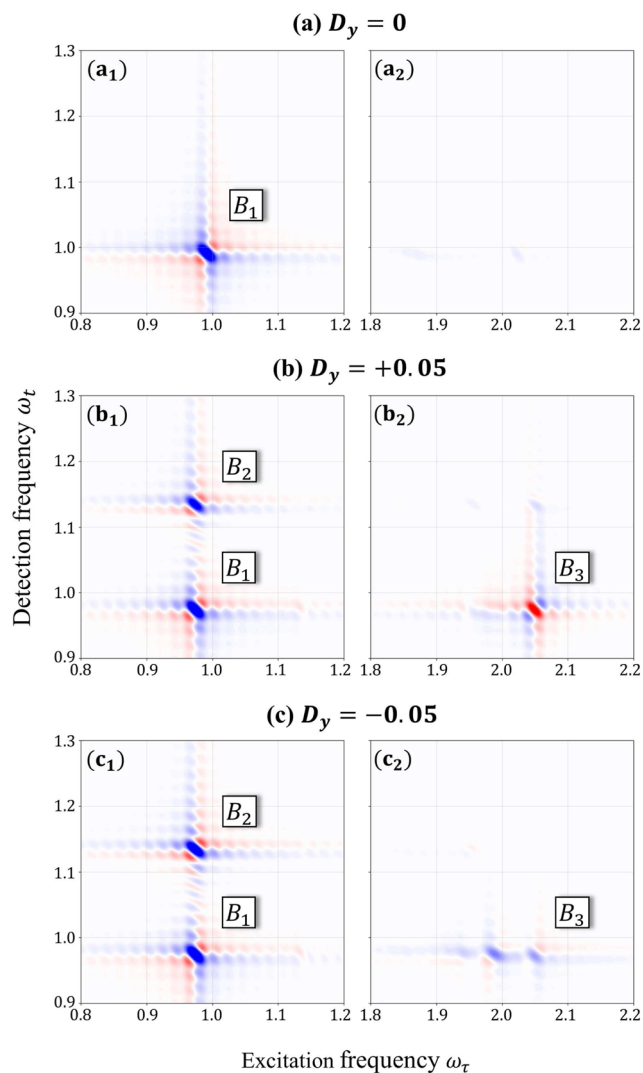

FIG. 3. 2D THz-MR spectrum calculated from $\chi_3^{(1)}(\omega_\tau, \omega_t)$ for three values of D_y: (a) 0, (b) +0.05, and (c) −0.05. The intensity of each spectrum is normalized with respect to its maximum peak intensity. The red and blue areas represent the positive and negative intensities of the spectra.

$|0_1\rangle \rightarrow |2_1\rangle \rightarrow |2_4\rangle \rightarrow |1_3\rangle$), while the right one evolves with time $\langle 0_1| \rightarrow \langle 1_3|$.[6,41]

The peaks labeled as B_1 and B_2 along $\omega_t = 0.98$ correspond to peaks A_1 and A_2 in the 1D spectra, and the frequency difference $\omega_{A_2} - \omega_{A_1}$ is equal to $\omega_{B_2} - \omega_{B_1}$. As illustrated in Fig. 4(a), diagrams B_1 and B_2 only involve the eigenstates that are (I) independent of the DMI and (II) dependent on the square of D_y. Thus, the intensities of the B_1 and B_2 peaks do not depend on the sign of D_y.

However, the $B_3^{(ii)}$ diagram in Fig. 4(a) involves states (II) and (III), while the $B_3^{(i)}$ diagram contains the state $|2_4\rangle$ that is (III) independent of the DMI but the phase of its wave function changes
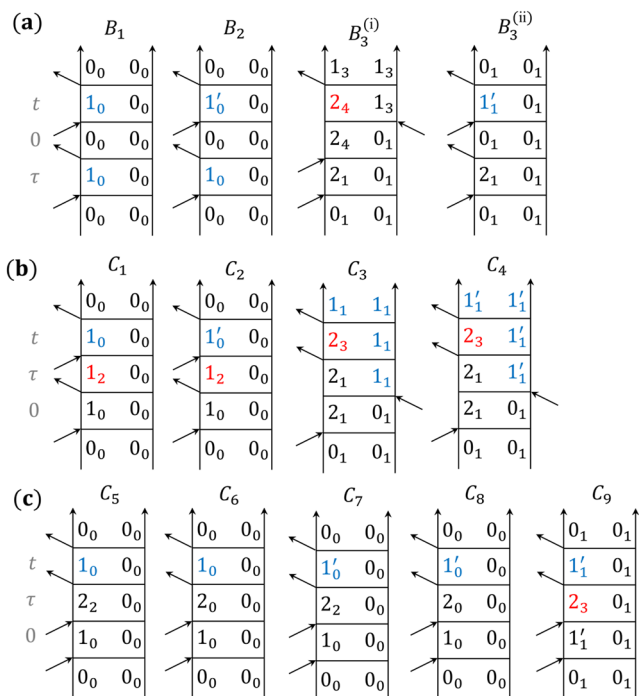
FIG. 4. (a)–(c) Double-sided Feynman diagrams for all labeled peaks. Two different contributions of B_3 are shown separately.

depending on the sign of D_y. As a result, the sign of the peak intensity changes for $D_y = +0.05$ and -0.05. However, the peak profiles in Figs. 3(b2) and 3(c2) are not positively and negatively symmetric due to the contribution from $B_3^{(ii)}$.

2. Contribution from $\chi_3^{(2)}(\omega_\tau, \omega_t)$

We next depict $\chi_3^{(2)}(\omega_\tau, \omega_t)$ in Fig. 5. Double-sided Feynman diagrams corresponding to each labeled peak are presented in Figs. 4(b) and 4(c).

Peaks C_1–C_4 appear in the case $D_y \neq 0$ because they involve the states classified in (II), as depicted in Fig. 4. Moreover, because peaks C_1–C_4 involve the $|1_2\rangle$ and $|2_3\rangle$ states classified in (III), in each of the diagrams in Fig. 4(b), the sign of the peak intensity changes in correspondence with the sign of D_y. Note that the peak profiles of C_1 for $D_y = 0$ and $D_y > 0$ are identical because the $|1_2\rangle$ state does not vanish even for $D_y = 0$. We also find that the positive peak near $(\omega_\tau, \omega_t) = (1.05, 1)$ in Fig. 5(a1) arises as the consequence of the heat-bath-induced coherence $|0_0\rangle\langle 1_0|$.

In Figs. 4(b2) and 4(c2), we observe that peaks C_5–C_9 arise from the 2Q coherence. Although the C_9 diagram involves the $|2_3\rangle$ state in (III), it overlaps with C_7 for $D_y \neq 0$, and the signs of the peak intensities cannot be easily evaluated. Note that here we chose a small system ($L = 6$) with periodic boundary conditions, so energy states higher than the second excited state are lowered, and the profiles of peaks C_5–C_9 are distorted. Hence, within the calculations of the present model, it is more reliable to use the profiles of C_1–C_4 to determine the sign of D_y.
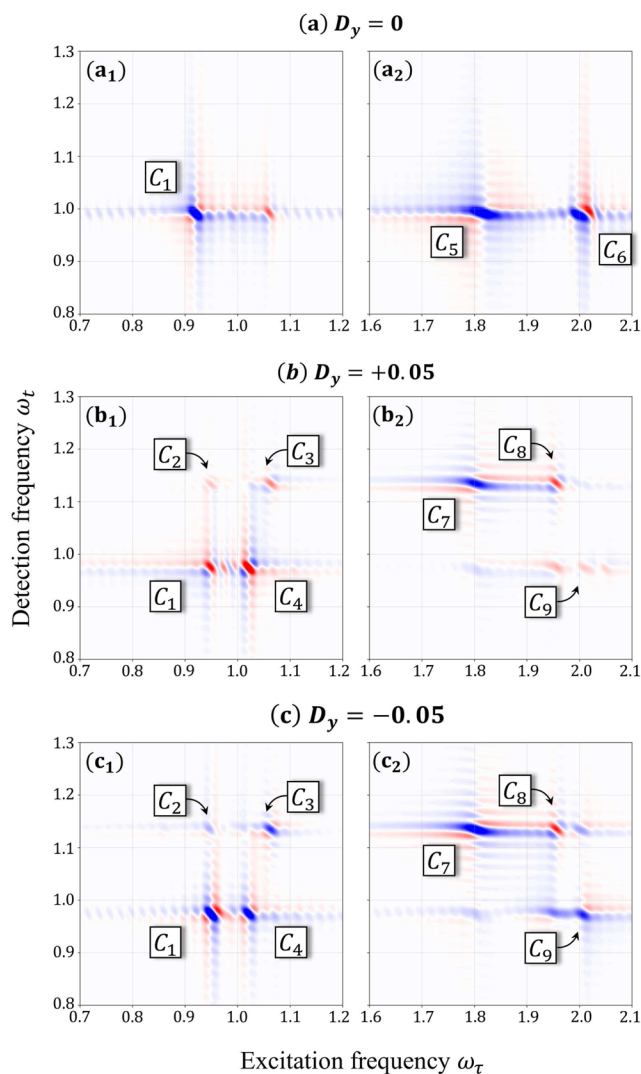
FIG. 5. 2D THz-MR spectrum calculated from $\chi_3^{(2)}(\omega_\tau, \omega_t)$ for three values of D_y: (a) 0, (b) +0.05, and (c) −0.05. The intensity of each spectrum is normalized with respect to its maximum peak intensity. The red and blue areas represent positive and negative intensities. All the parameter values are the same as those in Fig. 3.

V. CONCLUSION

A recently developed 2D THz-MR spectroscopic technique has created new possibilities for measuring complex molecular magnetic systems. In this work, we have illustrated the key features of this technique based on nonlinear response-function theory and have described a method for simulating 2D THz-MR spectra through the use of the HEOM formalism. Using simulated 1D and 2D THz-MR spectra for a chiral magnetic material, we demonstrated that the 2D technique allows us to evaluate the pitch and direction of chirality determined from the strength and sign of the DMI, while only the absolute amplitude of the DMI can be determined from 1D measurements.

06 July 2023 00:51:49

The reason that the sign of the DMI was detected by 2D spectroscopy in this study is that there are eigenstates in which the phase of the wavefunction changes following the sign of the DMI, which is categorized as (III). Although there have been studies of eigenstates of spin systems with the DMI,[58] the existence of eigenstates that change phase with the sign of the DMI, as found in this study, has not been explored. It is important to know the causes of these eigenstates because they may lead to the appearance of novel phenomena.

To make a direct comparison between the results of our simulations and those obtained experimentally, however, we must increase the number of spins in accordance with those available in experimental systems. In investigating spin dynamics in the condensed phase, it is also important to consider the non-perturbative and non-Markovian system–bath interactions. Nevertheless, we believe that the present results elucidate the key features of 2D THz-MR spectroscopic methods with regard to probing the fundamental nature of a magnetic spin system.

For further investigations to monitor the ultrafast dynamical aspects of the spin system, such as the dynamics of spin waves, it is necessary to conduct a variety of advanced nonlinear spectroscopic approaches, such as pump–probe and transient absorption measurements to foster the development of this spectroscopic method. We leave such extensions to future studies, depending on progress in experimental and simulation techniques.

AUTHOR DECLARATIONS

Conflict of Interest

The authors have no conflicts to disclose.

Author Contributions

Jiaji Zhang: Data curation (lead); Formal analysis (lead); Investigation (equal). **Yoshitaka Tanimura**: Conceptualization (lead); Funding acquisition (lead); Investigation (equal); Supervision (lead).

DATA AVAILABILITY

The data that support the findings of this study are available from the corresponding authors upon reasonable request.

REFERENCES

[1] J. Schraml and J. M. Bellama, *Two-Dimensional NMR Spectroscopy* (John Wiley & Sons, 1988).

[2] M. H. Levitt, *Spin Dynamics: Basics of Nuclear Magnetic Resonance* (John Wiley & Sons, 2013).

[3] T. J. Sato, D. Okuyama, T. Hong, A. Kikkawa, Y. Taguchi, T.-h. Arima, and Y. Tokura, "Magnon dispersion shift in the induced ferromagnetic phase of noncentrosymmetric MnSi," Phys. Rev. B **94**, 144420 (2016).

[4] J. Neu and C. A. Schmuttenmaer, "Tutorial: An introduction to terahertz time domain spectroscopy (THz-TDS)," J. Appl. Phys. **124**, 231101 (2018).

[5] Z. Zhang, F. Sekiguchi, T. Moriyama, S. C. Furuya, M. Sato, T. Satoh, Y. Mukai, K. Tanaka, T. Yamamoto, H. Kageyama, Y. Kanemitsu, and H. Hirori, "Generation of third-harmonic spin oscillation from strong spin precession induced by terahertz magnetic near fields," Nat. Commun. **14**, 1795 (2023).

[6] S. Mukamel, *Principles of Nonlinear Optical Spectroscopy*, Oxford Series in Optical and Imaging Sciences (Oxford University Press, 1995).

[7] G. F. Herrmann, "Resonance and high frequency susceptibility in canted antiferromagnetic substances," J. Phys. Chem. Solids **24**, 597–606 (1963).

[8] M. Nakajima, A. Namai, S. Ohkoshi, and T. Suemoto, "Ultrafast time domain demonstration of bulk magnetization precession at zero magnetic field ferromagnetic resonance induced by terahertz magnetic field," Opt. Express **18**, 18260–18268 (2010).

[9] K. Yamaguchi, M. Nakajima, and T. Suemoto, "Coherent control of spin precession motion with impulsive magnetic fields of half-cycle terahertz radiation," Phys. Rev. Lett. **105**, 237201 (2010).

[10] T. Kampfrath, A. Sell, G. Klatt, A. Pashkin, S. Mährlein, T. Dekorsy, M. Wolf, M. Fiebig, A. Leitenstorfer, and R. Huber, "Coherent terahertz control of antiferromagnetic spin waves," Nat. Photonics **5**, 31 (2011).

[11] T. Satoh, S.-J. Cho, R. Iida, T. Shimura, K. Kuroda, H. Ueda, Y. Ueda, B. A. Ivanov, F. Nori, and M. Fiebig, "Spin oscillations in antiferromagnetic NiO triggered by circularly polarized light," Phys. Rev. Lett. **105**, 077402 (2010).

[12] E. Turgut, A. Park, K. Nguyen, A. Moehle, D. A. Muller, and G. D. Fuchs, "Chiral magnetic excitations in FeGe films," Phys. Rev. B **95**, 134416 (2017).

[13] K. Dou, W. Du, Z. He, Y. Dai, B. Huang, and Y. Ma, "Theoretical prediction of antiferromagnetic skyrmion crystal in janus monolayer $CrSi_2N_2As_2$," ACS Nano **17**, 1144–1152 (2023).

[14] A. Soumyanarayanan, M. Raju, A. L. Gonzalez Oyarce, A. K. C. Tan, M.-Y. Im, A. P. Petrović, P. Ho, K. H. Khoo, M. Tran, C. K. Gan, F. Ernult, and C. Panagopoulos, "Tunable room-temperature magnetic skyrmions in Ir/Fe/Co/Pt multilayers," Nat. Mater. **16**, 898–904 (2017).

[15] M. Ozerov, J. Romhányi, M. Belesi, H. Berger, J.-P. Ansermet, J. van den Brink, J. Wosnitza, S. A. Zvyagin, and I. Rousochatzakis, "Establishing the fundamental magnetic interactions in the chiral skyrmionic Mott insulator Cu_2OSeO_3 by terahertz electron spin resonance," Phys. Rev. Lett. **113**, 157205 (2014).

[16] Y. Hayashi, Y. Okamura, N. Kanazawa, T. Yu, T. Koretsune, R. Arita, A. Tsukazaki, M. Ichikawa, M. Kawasaki, Y. Tokura, and Y. Takahashi, "Magneto-optical spectroscopy on Weyl nodes for anomalous and topological hall effects in chiral MnGe," Nat. Commun. **12**, 5974 (2021).

[17] K. Tsuruta, M. Mito, H. Deguchi, J. Kishine, Y. Kousaka, J. Akimitsu, and K. Inoue, "Nonlinear magnetic responses at the phase boundaries around helimagnetic and skyrmion lattice phases in MnSi: Evaluation of robustness of noncollinear spin texture," Phys. Rev. B **97**, 094411 (2018).

[18] T. Biesner, S. Roh, A. Pustogow, H. Zheng, J. F. Mitchell, and M. Dressel, "Magnetic terahertz resonances above the Néel temperature in the frustrated kagome antiferromagnet averievite," Phys. Rev. B **105**, L060410 (2022).

[19] L. Peedu, V. Kocsis, D. Szaller, B. Forrai, S. Bordács, I. Kézsmárki, J. Viirok, U. Nagel, B. Bernáth, D. L. Kamenskyi, A. Miyata, O. Portugall, Y. Tokunaga, Y. Tokura, Y. Taguchi, and T. Rõõm, "Terahertz spectroscopy of spin excitations in magnetoelectric $LiFePO_4$ in high magnetic fields," Phys. Rev. B **106**, 134413 (2022).

[20] K. Kozuki, T. Nagashima, and M. Hangyo, "Measurement of electron paramagnetic resonance using terahertz time-domain spectroscopy," Opt. Express **19**, 24950–24956 (2011).

[21] J. Lu, X. Li, H. Y. Hwang, B. K. Ofori-Okai, T. Kurihara, T. Suemoto, and K. A. Nelson, "Coherent two-dimensional terahertz magnetic resonance spectroscopy of collective spin waves," Phys. Rev. Lett. **118**, 207204 (2017).

[22] P. Hamm and M. T. Zanni, *Concepts and Methods of 2D Infrared Spectroscopy* (Cambridge University Press, 2011).

[23] M. Cho, *Two-Dimensional Optical Spectroscopy* (CRC Press, 2009).

[24] A. Fert, N. Reyren, and V. Cros, "Magnetic skyrmions: Advances in physics and potential applications," Nat. Rev. Mater. **2**, 17031 (2017).

[25] T. Jungwirth, X. Marti, P. Wadley, and J. Wunderlich, "Antiferromagnetic spintronics," Nat. Nanotechnol. **11**, 231–241 (2016).

[26]K. Inoue, "Chiral magnetism: Coupling static and dynamic chirality," Chem. Lett. **50**, 742–751 (2021).

[27]Y. Togawa, Y. Kousaka, K. Inoue, and J.-i. Kishine, "Symmetry, structure, and dynamics of monoaxial chiral magnets," J. Phys. Soc. Jpn. **85**, 112001 (2016).

[28]A. Kato, H. M. Yamamoto, and J.-i. Kishine, "Chirality-induced spin filtering in pseudo Jahn-Teller molecules," Phys. Rev. B **105**, 195117 (2022).

[29]J.-i. Kishine, K. Inoue, and Y. Yoshida, "Synthesis, structure and magnetic properties of chiral molecule-based magnets," Prog. Theor. Phys. Suppl. **159**, 82–95 (2005).

[30]P. Lodahl, S. Mahmoodian, S. Stobbe, A. Rauschenbeutel, P. Schneeweiss, J. Volz, H. Pichler, and P. Zoller, "Chiral quantum optics," Nature **541**, 473–480 (2017).

[31]M. Mito, K. Iriguchi, H. Deguchi, J.-i. Kishine, K. Kikuchi, H. Ohsumi, Y. Yoshida, and K. Inoue, "Giant nonlinear magnetic response in a molecule-based magnet," Phys. Rev. B **79**, 012406 (2009).

[32]Y. Okumura, F. Kagawa, S. Seki, M. Kubota, M. Kawasaki, and Y. Tokura, "Microwave magnetochiral dichroism in the chiral-lattice magnet Cu_2OSeO_3," Phys. Rev. Lett. **114**, 197202 (2015).

[33]E. M. Clements, R. Das, L. Li, P. J. Lampen-Kelley, M.-H. Phan, V. Keppens, D. Mandrus, and H. Srikanth, "Critical behavior and macroscopic phase diagram of the monoaxial chiral helimagnet $Cr_{1/3}NbS_2$," Sci. Rep. **7**, 6545 (2017).

[34]T. Nomura, X.-X. Zhang, S. Zherlitsyn, J. Wosnitza, Y. Tokura, N. Nagaosa, and S. Seki, "Phonon magnetochiral effect," Phys. Rev. Lett. **122**, 145901 (2019).

[35]A. G. Dijkstra and Y. Tanimura, "Non-Markovian entanglement dynamics in the presence of system-bath coherence," Phys. Rev. Lett. **104**, 250401 (2010).

[36]U. Weiss, *Quantum Dissipative Systems*, 4th ed. (World Scientific, 2012).

[37]H.-P. Breuer and F. Petruccione, *The Theory of Open Quantum Systems* (Oxford University Press, 2007).

[38]Y. Tanimura and R. Kubo, "Time evolution of a quantum system in contact with a nearly Gaussian-Markoffian noise bath," J. Phys. Soc. Jpn. **58**, 101–114 (1989).

[39]A. Ishizaki and Y. Tanimura, "Quantum dynamics of system strongly coupled to low-temperature colored noise bath: Reduced hierarchy equations approach," J. Phys. Soc. Jpn. **74**, 3131–3134 (2005).

[40]Y. Tanimura, "Stochastic Liouville, Langevin, Fokker–Planck, and master equation approaches to quantum dissipative systems," J. Phys. Soc. Jpn. **75**, 082001 (2006).

[41]Y. Tanimura, "Numerically 'exact' approach to open quantum dynamics: The hierarchical equations of motion (HEOM)," J. Chem. Phys. **153**, 020901 (2020).

[42]F. Bloch, "Nuclear induction," Phys. Rev. **70**, 460–474 (1946).

[43]A. G. Redfield, "The theory of relaxation processes," Adv. Magn. Opt. Reson. **1**, 1–32 (1965).

[44]R. Kubo, *Advances in Chemical Physics* (John Wiley and Sons, Ltd., 1969), pp. 101–127.

[45]T. Joutsuka and Y. Tanimura, "Detecting the Dzyaloshinskii-Moriya interaction by means of pulsed EPR spectroscopy," Chem. Phys. Lett. **457**, 237–240 (2008).

[46]H. Takahashi and Y. Tanimura, "Open quantum dynamics theory of spin relaxation: Application to μSR and low-field NMR spectroscopies," J. Phys. Soc. Jpn. **89**, 064710 (2020).

[47]Y. Wan and N. P. Armitage, "Resolving continua of fractional excitations by spinon echo in THz 2D coherent spectroscopy," Phys. Rev. Lett. **122**, 257401 (2019).

[48]P. Hamm and A. Shalit, "Perspective: Echoes in 2D-Raman-THz spectroscopy," J. Chem. Phys. **146**, 130901 (2017).

[49]T. Ikeda, H. Ito, and Y. Tanimura, "Analysis of 2D THz-Raman spectroscopy using a non-Markovian Brownian oscillator model with nonlinear system-bath interactions," J. Chem. Phys. **142**, 212421 (2015).

[50]F. Perakis, L. De Marco, A. Shalit, F. Tang, Z. R. Kann, T. D. Kühne, R. Torre, M. Bonn, and Y. Nagata, "Vibrational spectroscopy and dynamics of water," Chem. Rev. **116**, 7590–7607 (2016).

[51]H. Takahashi and Y. Tanimura, "Discretized hierarchical equations of motion in mixed Liouville–Wigner space for two-dimensional vibrational spectroscopies of liquid water," J. Chem. Phys. **158**, 044115 (2023).

[52]K. Reimann, M. Woerner, and T. Elsaesser, "Two-dimensional terahertz spectroscopy of condensed-phase molecular systems," J. Chem. Phys. **154**, 120901 (2021).

[53]K. Okumura and Y. Tanimura, "Two-dimensional THz spectroscopy of liquids: Non-linear vibrational response to a series of THz laser pulses," Chem. Phys. Lett. **295**, 298–304 (1998).

[54]J. Lu, Y. Zhang, H. Y. Hwang, B. K. Ofori-Okai, S. Fleischer, and K. A. Nelson, "Nonlinear two-dimensional terahertz photon echo and rotational spectroscopy in the gas phase," Proc. Natl. Acad. Sci. U. S. A. **113**, 11800–11805 (2016).

[55]Y. Iwamoto and Y. Tanimura, "Open quantum dynamics of a three-dimensional rotor calculated using a rotationally invariant system-bath Hamiltonian: Linear and two-dimensional rotational spectra," J. Chem. Phys. **151**, 044105 (2019).

[56]H.-B. Braun, J. Kulda, B. Roessli, D. Visser, K. W. Krämer, H.-U. Güdel, and P. Böni, "Emergence of soliton chirality in a quantum antiferromagnet," Nat. Phys. **1**, 159–163 (2005).

[57]H. Thoma, V. Hutanu, R. Dutta, A. Gukasov, V. Kocsis, Y. Tokunaga, Y. Taguchi, Y. Tokura, I. Kézsmárki, G. Roth, and M. Angst, "Magnetic order and sign of the Dzyaloshinskii-Moriya interaction in 2-D antiferromagnet $Ba_2CoGe_2O_7$ under applied magnetic field," IEEE Trans. Magn. **58**, 6400305 (2022).

[58]T. Sakai, O. Cépas, and T. Ziman, "An electron spin resonance selection rule for spin-gapped systems," J. Phys. Soc. Jpn. **69**, 3521–3524 (2000).

06 July 2023 00:51:49